The Astrophysical Journal, 971:35 (11pp), 2024 August 10 https://doi.org/10.3847/1538-4357/ad5722

Connections between Planetary Populations and Chemical Characteristics of Their Host Stars

Sol Yun[1], Young Sun Lee[2,3], Young Kwang Kim[2], Timothy C. Beers[3,4], Berfin Togay[1], and Dongwook Lim[5]
[1] Department of Astronomy, Space Science, and Geology, Chungnam National University, Daejeon 34134, Republic of Korea; yunsol719@gmail.com
[2] Department of Astronomy and Space Science, Chungnam National University, Daejeon 34134, Republic of Korea; youngsun@cnu.ac.kr
[3] Department of Physics and Astronomy, University of Notre Dame, Notre Dame, IN 46556, USA
[4] Joint Institute for Nuclear Astrophysics—Center for the Evolution of the Elements (JINA-CEE), USA
[5] Department of Astronomy, Yonsei University, Yonsei-ro, Seodaemun-gu, Seoul 03722, Republic of Korea
Received 2024 February 29; revised 2024 May 27; accepted 2024 June 10; published 2024 August 5

Abstract

Chemical anomalies in planet-hosting stars (PHSs) are studied in order to assess how the planetary nature and multiplicity affect the atmospheric chemical abundances of their host stars. We employ APOGEE DR17 to select thin-disk stars of the Milky Way, and crossmatch them with the Kepler Input Catalog to identify confirmed PHSs, which results in 227 PHSs with available chemical abundance ratios for six refractory elements. We also examine an ensemble of stars without planet signals, which are equivalent to the selected PHSs in terms of evolutionary stage and stellar parameters, to correct for Galactic chemical evolution effects, and derive the abundance gradient of refractory elements over the condensation temperature for the PHSs. Using the Galactic chemical evolution corrected abundances, we find that our PHSs do not show a significant difference in abundance slope from the stars without planets. However, when we examine the trends of the refractory elements of PHSs, based on the total number of their planets and their planet types, we find that the PHSs with giant planets are more depleted in refractory elements than those with rocky planets. Among the PHSs with rocky planets, the refractory depletion trends are potentially correlated with the terrestrial planets' radii and multiplicity. In the cases of PHSs with giant planets, sub-Jovian PHSs demonstrate more depleted refractory trends than stars hosting Jovian-mass planets, raising questions on different planetary formation processes for Neptune-like and Jupiter-like planets.

Unified Astronomy Thesaurus concepts: Star-planet interactions (2177); Planetary system formation (1257); Chemical abundances (224); Stellar abundances (1577); Stellar kinematics (1608); Galaxy chemical evolution (580)

1. Introduction

A star and its planets are thought to have formed from the same molecular cloud. The composition of a star could influence the protoplanetary disk where planets form, and the accreting material from the protoplanetary disk onto the host star may be chemically imprinted in the atmosphere of the star. These interactions may result in an intricate relationship between the chemical composition of a star and the formation and evolution of its planets. Various approaches have been conducted to find such connections between the chemical composition of a planet-hosting star (PHS) and its planet formation and architecture. Notably, the amount of heavy elements in a stellar atmosphere, often characterized by metallicity ([Fe/H]), has received attention due to its expected implications for the occurrence and properties of planetary companions (e.g., Gonzalez 1997; Heiter & Luck 2003; Santos et al. 2004; Fischer & Valenti 2005; Udry & Santos 2007; Adibekyan et al. 2012a).

Meléndez et al. (2009) first reported, based on an analysis of 11 solar twin stars, that the Sun's refractory elements (Mg, Al, Si, etc.), which have condensation temperatures (T_C) over 1200 K, are relatively depleted compared to those of the volatile elements (C, N, O, etc.). They suggested that refractory depletion is correlated with the presence of terrestrial planets; the material to form the rocky planet readily incorporates elements with high T_C in the solid phase, while the low T_C volatile elements likely remain in the gas phase. This was further supported by Chambers (2010), who claimed that the deficit of the refractory elements in the solar photosphere could account for roughly 4 $M_\oplus$ of terrestrial material. These studies have triggered numerous efforts to identify differences in the chemical abundances between PHSs and non-PHSs (NPHSs) using chemical abundance trends as a function of condensation temperature (e.g., Ramírez et al. 2009; González Hernández et al. 2011, 2013; Adibekyan et al. 2014; Nissen 2015; Bedell et al. 2018; Liu et al. 2020; Nibauer et al. 2021; Tautvaišienė et al. 2022).

When investigating the chemical abundance trends of a star, one also needs to carefully take into account how Galactic chemical evolution (GCE) affects the chemical abundance pattern. Bedell et al. (2018) identified the relative depletion of refractory elements from an analysis of 26 elements for 79 solar twins. At the same time, they recognized that some of the depletion trend may be caused by GCE. They further demonstrated that the depletion trend is real, after carefully correcting for the GCE effects in their Sun-like stars. Such a study indicates that the GCE correction is a vital step when comparing stars with different ages but similar metallicity and temperatures (e.g., Gibson et al. 2003; Spina et al. 2016, 2018; Pignatari et al. 2023). Other studies (Adibekyan et al. 2014; Nissen 2015; Spina et al. 2016) also show that a careful selection of the comparison stars with similar stellar parameters is crucial, due to the presence of correlations between stellar

parameters and chemical abundance patterns before the application of the GCE correction. As the GCE correction is nontrivial, in order to minimize systematic uncertainties resulting from GCE (and adopted stellar models) several studies focused their attention on wide binaries whose evolutionary states are nearly identical, so that these effects are not significant for the analysis (e.g., Liu et al. 2014, 2021; Tucci Maia et al. 2014; Ramírez et al. 2015; Saffe et al. 2015; Teske et al. 2016; Oh et al. 2018; Biazzo et al. 2022).

In spite of great progress, the chemical anomalies observed in the Sun relative to solar twins have not been consistently confirmed as a unique feature in other studies (e.g., Gonzalez et al. 2010; Meléndez et al. 2012; González Hernández et al. 2013; Nissen 2015; Liu et al. 2020; Nissen et al. 2020; Nibauer et al. 2021). Additionally, studies that examined the relationship between stellar chemical anomalies and planet formation were not successful in detecting a definitive signal of such a relationship, and triggered more controversy (Adibekyan et al. 2014; Liu et al. 2020; Tautvaišienė et al. 2022; Behmard et al. 2023). Nibauer et al. (2021), for instance, found two groups of stars: chemically depleted and nondepleted ones, by introducing a likelihood-based approach to determine elemental abundances in solar analog stars identified in Apache Point Observatory Galactic Evolution Experiment Data Release 16 (APOGEE DR16; Jönsson et al. 2020). They agreed on the refractory depletion of the Sun with Bedell et al. (2018), arguing that the Sun is one of the stars in their refractory-depleted group.

Similarly, Liu et al. (2020) analyzed 16 PHSs and 68 comparative NPHSs, following the methods of Bedell et al. (2018), and found various abundance–T_C trends among PHSs without a clear signature of the depletion of the refractory elements for the PHSs. They suggested that a range of possible planet-induced effects are responsible. Behmard et al. (2023) carried out a study on the chemical dissimilarity of 12 elements between 130 known/candidate Kepler objects of interest (KOIs) of PHSs and so-called doppelgängers stars, selected based on the proximity of four parameters: effective temperature ($T_{\rm eff}$), surface gravity ($\log g$), [Fe/H], and [Mg/H] in high-resolution near-infrared spectra from APOGEE DR17 (Abdurro'uf et al. 2022). They reported that the median intrinsic dispersion between the KOI and doppelgänger samples was consistently under 0.05 dex, and argued that there are no noticeable signatures for different chemical abundance patterns associated with PHSs.

Based on the studies to date, a consensus on the connection between the chemical properties of a PHS and its planet formation history has yet to be achieved, nor have any clear differences in the chemical properties between PHSs and NPHSs been identified. This leads us to investigate how the planet population (number of planets and their types, often referred to as the "architecture" of a planetary system) affects the chemical abundance patterns of its host star, which has not been thoroughly explored previously. To achieve this goal, we employ a large sample of stars from APOGEE DR17 with well-determined stellar parameters and chemical abundances.

This paper is arranged as follows. In Section 2, we identify dwarfs and subgiants that are likely members of the Galactic thin disk, based on their chemical and kinematic properties. We confirm the stars that are PHSs and NPHSs by crossmatching the APOGEE sample with the Kepler Input Catalog (KIC) and Kepler catalogs, respectively. We also identify likely twin stars within these subsamples. We apply GCE corrections to both subsamples in Section 3. Section 4 presents the abundance trends as a function of T_C for the PHSs. In Section 5, we present the results of our detailed analysis of the overall trends of the abundance slopes between the terrestrial planets and the Jovian planets. In addition, we consider the dependency of chemical abundance depletion on the nature of the host's planet population. We discuss the implications of our findings regarding planet architecture, along with those of other studies, in Section 6. A summary and conclusions are provided in Section 7.

2. Data

2.1. Identification of Thin-disk Stars

To identify a star with planets, we first selected likely thin-disk stars of the Milky Way (MW) of various chemical abundances, using the large spectroscopic survey data from APOGEE DR17 (Abdurro'uf et al. 2022). APOGEE DR17 provides high-resolution ($R\sim22{,}500$) spectra in the H band across the MW. The stellar parameters and abundance ratios for numerous chemical elements in these spectra are delivered by the APOGEE Stellar Parameters and Abundances Pipeline (García Pérez et al. 2016).

We computed the space-velocity components and orbital parameters of the APOGEE stars using astrometric data from Gaia Data Release 3 (Gaia DR3; Gaia Collaboration et al. 2023) and a Stäckel-type potential, as employed in several previous studies (e.g., Chiba & Beers 2000; Kim et al. 2019, 2021, 2023; Lee et al. 2019, 2023; Kang et al. 2023). For these calculations, we adopted a local standard of rest velocity ($V_{\rm LSR}=236\,{\rm km\,s^{-1}}$; Kawata et al. 2019), a solar location of $R_\odot=8.2\,{\rm kpc}$ and $Z_\odot=20.8\,{\rm pc}$ from Bland-Hawthorn & Gerhard (2016) and Bennett & Bovy (2019), respectively, and a solar peculiar motion $(U,\ V,\ W)_\odot=(-11.10,\ 12.24,\ 7.25)\,{\rm km\,s^{-1}}$ (Schönrich et al. 2010). Among the orbital parameters, we derived $Z_{\rm max}$ (maximum distance from the Galactic plane), which is often used as one of the criteria for the selection of disk stars. Additionally, we calculated $R_{\rm max}$ and $R_{\rm min}$, which are maximum and minimum distances, respectively, from the Galactic center projected onto the Galactic plane. We applied the –0.017 mas systematic offset reported in Gaia DR3 (Lindegren et al. 2021) when calculating the distances.

To select the disk-star population, we imposed the following criteria: $3100\leqslant T_{\rm eff}\leqslant6500\,{\rm K}$, $\log g\geqslant3.5$, $[{\rm Fe/H}]>-1.2$, $7\leqslant R\leqslant11\,{\rm kpc}$, $d<4\,{\rm kpc}$, $Z_{\rm max}<3\,{\rm kpc}$, signal-to-noise ratio ${\rm (S/N)}>50$, $V_\phi>50\,{\rm km\,s^{-1}}$, $V_Z<100\,{\rm km\,s^{-1}}$, and relative parallax error less than 20%. R is the distance from the Galactic center projected onto the Galactic plane, d is the heliocentric distance, V_ϕ is the rotational velocity, and V_Z is the vertical velocity component. Then, the identification of likely thin-disk members was conducted following the methodology of Han et al. (2020), who used both chemical abundances ([Fe/H] and [α/Fe]) and kinematics to derive the membership probability of each star. Note that, in this study, we attempt to analyze PHSs in the Galactic thin disk because the thin-disk stars generally do not exhibit chemical peculiarities, unlike the thick-disk and halo stars. Additionally, we excluded in our program stars the likely accreted stars, whose origins and natures are not similar to the canonical disk stars. Following the chemical criteria of Belokurov & Kravtsov (2022), we identified 30,265 stars with

[Fe/H] < –0.4 and [Al/Fe] < –0.075 as accreted objects. These various selection criteria left us with 101,393 dwarf stars likely to belong to the MW's thin disk.

2.2. Chemical Elements

We now characterize PHSs through an examination of their chemical abundance trends. Among the abundance ratios of 18 elements made available in APOGEE DR17, we employed those with elemental abundances having uncertainties that are sufficiently small to achieve the sensitivity required to detect abundance trends as a function of T_C (Lodders 2003) in a star; less than 0.03 dex, as demonstrated in previous studies (Adibekyan et al. 2012b; Bedell et al. 2014; Liu et al. 2020; Nibauer et al. 2021). We chose six refractory elements (Mg, Al, Si, Ca, Mn, and Ni) with the following conditions in mind. First, their T_C is over 1000 K, the lowest temperature of the refractory elements (Meléndez et al. 2009; Ramírez et al. 2009; Liu et al. 2020). Second, their absolute abundance errors are less than 0.02 dex, with no flags raised in *X FE FLAG* for each element. Third, they are key elements for studying and testing planet formation scenarios (McDonough & Sun 1995; Wang et al. 2022). These conditions allowed us to select 47,988 stars from our thin-disk candidate stars with well-determined abundances of Mg, Al, Si, Ca, Mn, and Ni. We did not include the abundances for the volatile elements because their relatively larger abundance errors in APOGEE DR17 make their abundance–T_C trends uncertain.

2.3. PHSs and Their Twins

2.3.1. Selection of PHSs

We identify PHSs by crossmatching our selected thin-disk stars from APOGEE DR17 with the KIC Data Release 10 (Brown et al. 2011) and the cumulative catalog of KOI in the NASA Exoplanet Archive.[6] Within the catalog provided on the NASA Exoplanet Archive website, we used the PHS data with "koi_disposition = Confirmed" to avoid any confusion between the other stellar and planetary signals from various sources. Furthermore, we compiled the planetary parameters, such as the planetary radius, of the selected PHS samples from the confirmed planet catalog (published on 2023 October 18) with "default_flag = 1," resulting in a sample of 283 stars hosting 423 planets.

Similarly, we selected 2356 comparison stars by crossmatching with the Kepler data without planetary signatures, which we take to be NPHSs, after excluding 142 stars with candidate flags. Once again, we crossmatched our data with the TESS Object of Interest (Guerrero et al. 2021) candidate list to make sure of the absence of any possible planetary signals in our comparison sample. This sample is used for selecting the twin stars of the PHSs, as described below.

2.3.2. Selection of Twins for PHSs

To search for chemical distinctions among PHSs, we require a sample of stars without planets to compare with, and used to correct for GCE effects. It is also necessary for them to be in similar evolutionary stages and metallicities to the PHSs. However, it is extremely difficult and time-consuming to identify the NPHSs that are exact counterparts of the PHSs. Following the work of Nibauer et al. (2021) and Behmard et al. (2023), we employ *twins* of the PHSs (TPHSs), which are similar spectral types and luminosity classes to their counterpart PHSs.

The definition of a stellar twin is diverse in the literature. In order to demonstrate the depletion of the Sun's refractory elements with respect to volatile elements, Meléndez et al. (2009) considered as solar twins the stars with $T_{\rm eff}$, $\log g$, and [Fe/H] are less than 75 K, 0.1 dex, and 0.07 dex, respectively from those of the Sun, $T_{\rm eff} = 5777$ K, $\log g = 4.44$, and [Fe/H] = 0.0. Similarly, Ramírez et al. (2009) and Bedell et al. (2018) adopted the criteria of Δ100 K in $T_{\rm eff}$, Δ0.1 dex in $\log g$, and Δ0.1 dex in [Fe/H] to select solar twins, while Berke et al. (2023) used the condition of Δ100 K in $T_{\rm eff}$, Δ0.2 dex in $\log g$, and Δ0.1 dex in [Fe/H]. In contrast, Liu et al. (2020) considered only effective temperature and metallicity to increase the number of solar analogs, while Behmard et al. (2023) introduced [Mg/H] as an additional criterion to evaluate the similarities among their stars.

Having reviewed the selection criteria used in previous studies, among the NPHSs identified in Section 2.3.1, we sorted out the TPHSs by adopting the "twin regions" of Δ100 K in $T_{\rm eff}$, Δ0.1 dex in $\log g$, and Δ0.1 dex in [Fe/H] from the parameters of each PHS to closely match their evolutionary states. Each PHS in our sample has, on average, 43 TPHSs within their twin regions. We further confirmed that the selected TPHSs have close proximity to the target PHS by enforcing the total distance of the parameters to the minimum in a χ^2 fashion, as employed by Behmard et al. (2023):

$$D^2 = \left(\frac{T_{{\rm eff}P} - T_{{\rm eff}T}}{\sqrt{\sigma^2_{T_{{\rm eff}P}} + \sigma^2_{T_{{\rm eff}T}}}}\right)^2 + \left(\frac{\log g_P - \log g_T}{\sqrt{\sigma^2_{\log gP} + \sigma^2_{\log gT}}}\right)^2 + \left(\frac{[{\rm Fe/H}]_P - [{\rm Fe/H}]_T}{\sqrt{\sigma^2_{[{\rm Fe/H}]P} + \sigma^2_{[{\rm Fe/H}]T}}}\right)^2, \quad (1)$$

where P indicates a PHS, and T is the twin of a PHS. We only used the first 20 TPHSs with the smallest D^2 value for further analysis.

Of 283 PHSs, 40 stars have less than 20 TPHSs, with 12 TPHSs on average within their twin regions. When relaxing the selection criteria of TPHS to include up to 20 TPHSs for those PHSs, their stellar parameters significantly vary, ranging from Δ0.6 dex in [Fe/H] and Δ1.0 dex in $\log g$, which is far from our definition of the twins. We thus excluded these 40 stars from our analysis, leaving 243 PHSs hosting 397 planets in total.

3. Corrections for GCE

Previous studies recognized that corrections for GCE are a crucial step for accurately evaluating the abundance trend of PHSs in the abundance–T_C plane (Adibekyan et al. 2014; Spina et al. 2016; Bedell et al. 2018). GCE refers to how chemical elements formed and were distributed in the MW (Gibson et al. 2003; Spina et al. 2016; Pignatari et al. 2023). The formation rate and the amount of elements created vary depending on the star formation rate and initial mass function. For instance, our target elements, Mg, Si, and Ca, which are often called "alpha elements," are mostly created during massive-star evolution and distributed into the interstellar medium (ISM) by Type II

[6] https://exoplanetarchive.ipac.caltech.edu/

supernovae (SNe), while Mn and Ni (iron-peak elements) are formed during the explosion of Type Ia SNe, an event involving relatively low-mass stars. Since the timescales for these progenitors differ, depending on how the ISM has been chemically enriched, a star formed out of the ISM exhibits a distinctive chemical abundance pattern that can vary from star to star according to its age. To elucidate the chemical trend that represents the stellar birth environment, we need to remove the stochastic variation of chemical abundances caused by chemical evolution. This is known as the "GCE correction."

Stellar age is a crucial parameter for the GCE correction. In this regard, some studies (Bedell et al. 2018; Liu et al. 2020) excluded alpha-enhanced, old thick-disk stars from estimating GCE effects. However, we do not exclude stars older than 10 Gyr, because our samples are selected as likely thin-disk stars based on their chemical and kinematic properties. Moreover, we did not find old stars whose abundances of the six refractory elements significantly deviated from the main abundance trend of relatively younger stars, which was the primary reason for excluding the old stars in other studies. Nonetheless, to ensure the accuracy of our stellar ages, we eliminated the stars whose age errors are larger than 3 Gyr in the catalog provided by Mackereth et al. (2019). The stellar ages reported in this catalog are determined by the astroNN[7] package, and it includes asteroseismic ages from APOKASC-2 (Pinsonneault et al. 2018) and low-metallicity asteroseismic ages (Montalbán et al. 2021). This additional age constraint leaves us with 227 PHSs and 2344 TPHSs with well-determined ages.

Most of previous studies corrected for GCE by subtracting the abundance trend of each element with respect to the stellar age (Nissen 2015, 2016; Bedell et al. 2018; Spina et al. 2018; Liu et al. 2020; Nissen et al. 2020). Similarly, we attempted to correct for it by following the methodology of Spina et al. (2016) and Nissen et al. (2020). We derived a best linear fit to each element as a function of stellar age using the 20 TPHS samples for each PHS. We did not include PHSs when deriving the linear fit because of the possibility of stellar abundance variations associated with the existence of planets. The measured slope (m) and intercept (b) of each element were applied to correct for GCE effects in the following manner:

$$[\mathrm{X/Fe}]_{\mathrm{correct}} = [\mathrm{X/Fe}]_{\mathrm{raw}} - (m \times \mathrm{age} + b), \quad (2)$$

where X represents each element.

Note that, unlike the previous studies, we did not attempt to homogeneously apply the same GCE correcting parameter (m, b) to all samples. Rather, we calculated the GCE correction parameter for individual PHSs separately, using the TPHSs selected for each PHS, and then applied the slope and intercept to correct the GCE for each PHS. We believe that our GCE correction more clearly reflects the evolution effects of PHS by using TPHSs, which have similar atmospheric parameters with PHS within various age ranges.

For the Sun, the values of the GCE correction parameters did not change significantly by varying the choice of the selected TPHS number from 10 to 30. We also found that the Sun's abundance trend against T_{C} was nearly identical regardless of the selected number of TPHSs. For the PHS sample, however, we found that the abundances of Al and Mn after GCE correction changed significantly when we decreased the TPHS number from 20 to 10, but not when it was increased from 20 to 30 TPHSs for each PHS. This is the main reason for choosing 20 TPHS. We corrected the GCE effect for each TPHS in the same way as well, using the selected TPHSs of each PHS.

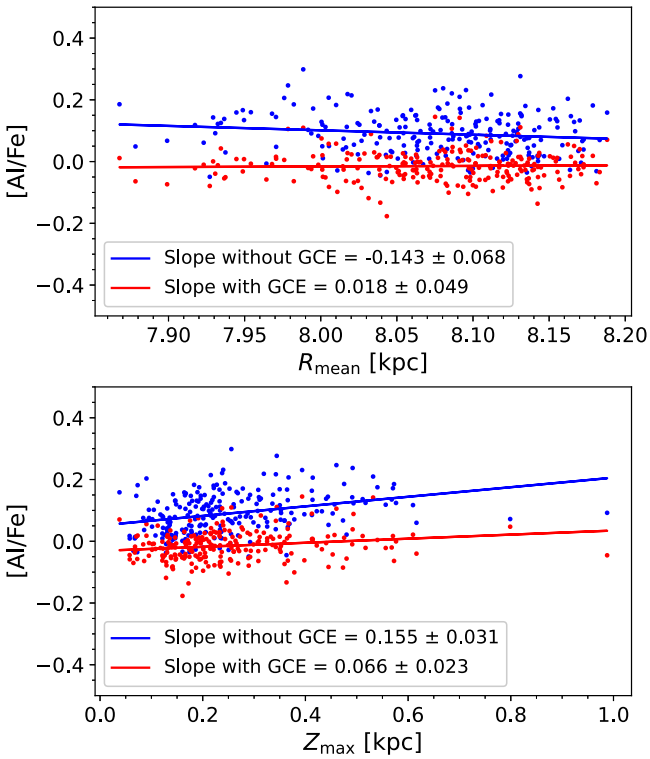

Figure 1. Aluminum abundance ratios of our PHSs, as a function of R_{mean} (upper panel) and Z_{max} (lower panel). The blue and red dots represent the abundance ratios before and after GCE correction, respectively. The colored solid lines are the fitted trends. The derived slopes and errors in the slopes are denoted at the lower left corner of each panel.

Because stars could form in gas clouds that experience different chemical evolution, which could vary with distance from the Galactic center and plane, we also examined the abundance trends over R_{mean} ($=(R_{\mathrm{max}} + R_{\mathrm{min}})/2$) and Z_{max}. Figure 1 shows the [Al/Fe] abundance ratios, as functions of R_{mean} (top panel) and Z_{max} (bottom panel). The blue and red dots represent the ratios before and after GCE correction, respectively. The colored solid lines are the fitted trends. The derived slopes and errors are denoted at the lower left corner of each panel. As we selected our sample stars in the Kepler field, our PHSs cover a very narrow range of R_{mean} and Z_{max}. Even though there is a noticeable slope (blue line), after the GCE correction the abundance gradient becomes insignificant. We checked the abundance slopes for other elements, and found that the magnitudes of their abundance gradients are much smaller after the GCE correction than that of the [Al/Fe] ratio. We derived a simple abundance correction function with respect to R_{mean} and Z_{max}, similar to Equation (2), and applied it to remove the abundance trend of each PHS at its location. We found that our derived abundance–T_{C} slopes are consistent with those that are only corrected for the GCE effect. These results suggest that the abundance ratio trends with R_{mean} and Z_{max} do not greatly affect the derivation of the abundance slope over T_{C}. Therefore, we do not apply additional corrections to the elemental abundances with respect to R_{mean} and Z_{max}, beyond the GCE correction.

[7] https://github.com/henrysky/astroNN

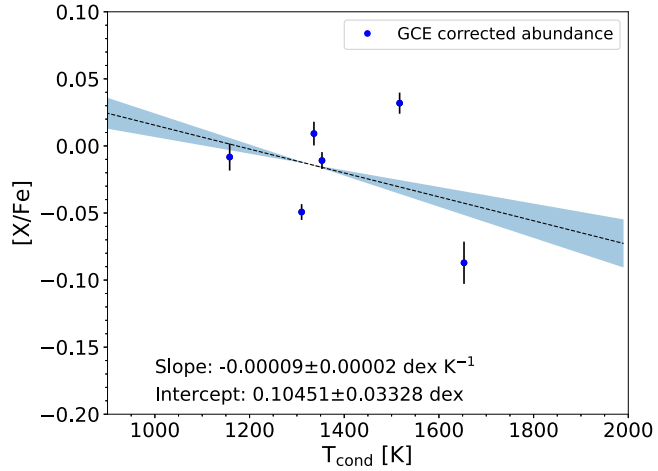

Figure 2. Sun's GCE-corrected abundance trend as a function of T_C. Each dot represents the six elements (Mn, Si, Mg, Ni, Ca, and Al in order of T_C) placed at corresponding T_C, with error bars indicating the 1σ of abundance value measured by 1000 random resamplings of the TPHSs, while correcting for GCE effects. The black dashed line is the best-fit line, with the blue-shaded region displaying the 1σ of the slopes. The derived slope, intercept, and their 1σ values are indicated in the legend.

4. Derivation of the Abundance–T_C Slope

We employed the method of the abundance gradient over T_C, which is the most widely used one to identify the chemical depletion or enhancement in a star. We have learned from previous studies that the accuracy of the chemical abundances of the PHSs plays a pivotal role in drawing a robust abundance slope over T_C. At the same time, it is imperative that the comparison sample (TPHSs in our case) accurately reflects the evolutionary stage of their counterparts as closely as possible. To robustly detect the variation of the abundance ratios, we made use of high-T_C refractory elements with the most reliable abundance determinations, as reported in Jönsson et al. (2020). These are Mg, Al, Si, Ca, Mn, and Ni. We did not include volatile elements with T_C under 900 K because they fall outside the steepest portion of the depletion trend (Meléndez et al. 2009; Chambers 2010; Bedell et al. 2018).

Figure 2 shows an example of the derived abundance trend as a function of T_C. The figure shows the abundance slope of refractory elements of the Sun after the GCE correction. Each dot represents the six elements (Mn, Si, Mg, Ni, Ca, and Al in order of T_C) placed at their corresponding T_C; error bars were calculated from 1000 random resamplings of the Sun's twins while correcting for GCE. The dotted line is the abundance gradient derived from linear fit to the six elemental abundances. The blue-shaded region shows the 1σ variation of the slope values, and the figure clearly indicates that the Sun is deficient with the refractory elements after the GCE correction.

Other studies also reported the depletion of refractory elements in the Sun. For instance, Bedell et al. (2018) analyzed 79 solar twins to find evidence of the depletion of 26 elements in the Sun after the GCE correction. Similarly, Liu et al. (2020) demonstrated that the Sun's refractory elements are relatively depleted compared to its analog stars. Nibauer et al. (2021) successfully reproduced the results of Bedell et al. (2018) using only five refractory elements from APOGEE DR16 (Jönsson et al. 2020), supporting the depletion argument.

Using six refractory elements from APOGEE DR17, we reach the same conclusion. Note that our approach is somewhat different from the previous studies, in that our abundance slope is not derived from the star-to-star abundance differences between the PHSs and NPHSs, as done in most of the other studies (Meléndez et al. 2009; Bedell et al. 2018; Liu et al. 2020; Nibauer et al. 2021; Tautvaišienė et al. 2022). Instead, the derived slope value represents the trends of the Sun's abundance values after correction of the chemical evolution of the MW.

5. Results

5.1. Distribution of Abundance–T_C Slopes

The primary reasons for the depletion of the Sun's refractory elements are still under discussion. Meléndez et al. (2009) argued that this depletion arose due to the presence of rocky planets such as Earth (see Haxton & Serenelli 2008 for another view). However, other studies (González Hernández et al. 2013; Liu et al. 2020; Mishenina et al. 2021) failed to find evidence to support this hypothesis, even with much higher-quality abundance analyses for limited samples. Extending the idea to other planetary systems, some studies reported a weak correlation between planetary mass and stellar chemical abundance (Mishenina et al. 2021; Tautvaišienė et al. 2022), while others using large survey data concluded that there is no clear sign of the correlation resulting from the existence of planets (Nibauer et al. 2021; Behmard et al. 2023).

Based on our much larger sample of PHSs and TPHSs, we have investigated these issues by comparing the abundance–T_C slopes of PHSs with those of the TPHSs (stars without planetary detections), as shown in Figure 3. The abundance–T_C slopes of TPHSs are measured in the same manner as for the PHSs, using 20 TPHSs for each TPHS. In the figure, the orange lines represent the distribution of the PHSs and the blue lines are for the TPHSs. The left panel is before the GCE correction, while the right panel is after the GCE correction.

A comparison of the two panels in Figure 3 reveals that the GCE-corrected samples exhibit a consistently greater fraction of negative slopes, indicating that the GCE correction is an important step to apply when examining any abundance depletion or enhancement. Inspection of the right panel suggests that the PHSs do not exhibit a significant difference in the distribution of slopes from the TPHSs, although we observe a small enhancement of relative numbers of stars around the slope of -2.0×10^{-4} dex K^{-1} for the PHSs, which was not observed before the GCE correction. We conclude that the existence of planetary systems does not strongly influence the chemical properties of their host stars, as pointed out by previous studies. To quantitatively evaluate the significance of the difference in the distributions, we carried out a Kolmogorov–Smirnov (K-S) two-sample test under the null hypothesis that the two groups of stars share the same parent chemical properties. From the distribution with the GCE correction (right panel), we obtained a p-value of 0.1, implying that we cannot rule out the null hypothesis completely. We have thus focused on the existence of any chemical discrepancies among the PHSs with different planet populations and architectures.

5.2. Terrestrial versus Jovian Planets

Before exploring how the different types of planets affect the chemical characteristics of their host stars, we need to distinguish the terrestrial planets from the Jovian planets by considering their observables such as mass and radius. Most recent studies, such as Mishenina et al. (2021) and Tautvaišienė

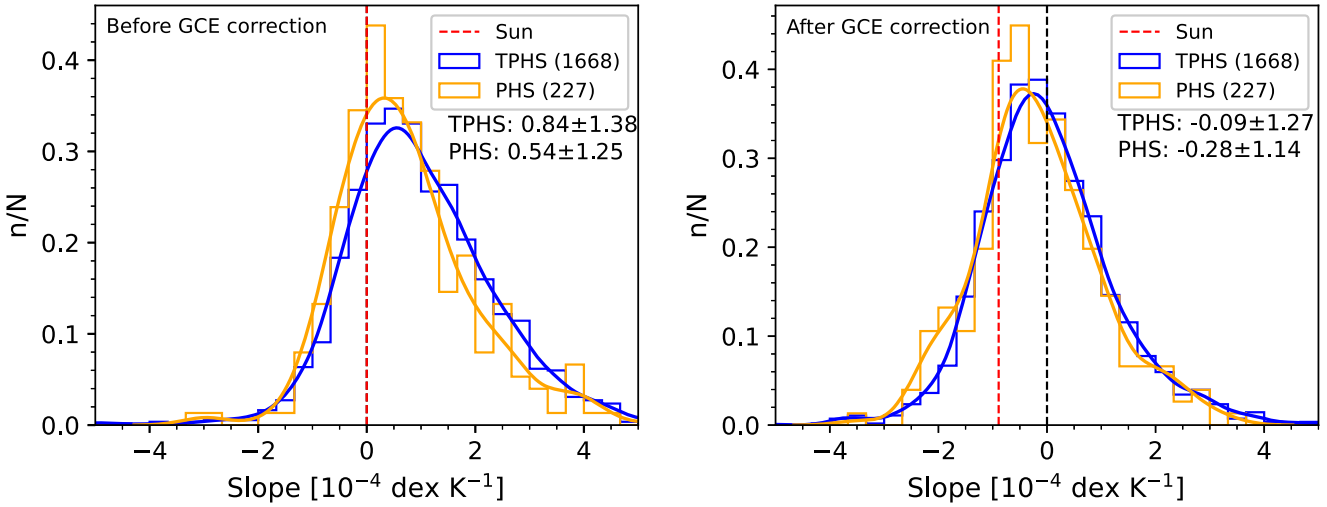

Figure 3. Distributions of the abundance–T_C slopes for our PHSs (orange) and TPHSs (blue). The left panel represents the results before the GCE correction, while the right panel is after the GCE correction. The smoothed distribution is a KDE. The median slope and 1σ value for each group are denoted in each panel. The red and black dashed vertical lines are the solar slope and zero-point, respectively. The distribution is normalized to the total number of stars in each group.

et al. (2022), attempted to correlate the planetary system properties with the chemical composition of their host stars by the use of the planetary mass. Out of the 338 planets in our sample, only 80 have known mass information, while the radius information is available for 323 planets, determined by transit observations. Since more planets provide more robust statistics, we decided to use the planetary radius information to distinguish the terrestrial from the Jovian planets, and examine any connection to the abundance patterns of their host stars. We used a total of 216 PHSs with known planets and their radii.

No super-Earth located at larger than $3\,R_\oplus$ has been found to date, and according to the planetary orbital period–radius diagram, the Neptune desert spans from 2 to $10\,R_\oplus$ with an orbital period of less than 10 days. Referring to these two observational constraints, we decided to set the distinguishing criterion at $3\,R_\oplus$ between rocky and gas giant planets. If the mean radius (R_M) of all known planets in a planetary system is less than $3\,R_\oplus$, we assume that the system is dominated by terrestrial planets, and by gas giants for $R_M \geqslant 3\,R_\oplus$. It should be noted that our dividing condition for the types of planets is not an absolute standard, and is subject to change as more diverse planetary systems are discovered in different environments. Our sample comprises 155 single planetary systems and 61 multiple planetary systems.

To gain a deeper understanding of how the formation of different types of planets (e.g., rocky versus gaseous) influences the chemistry of their host stars, once again we derived the abundance slope of the refractory elements over T_C for the subgroups of PHSs with terrestrial or Jovian planetary systems. Figure 4 presents these distributions. The blue histogram represents the terrestrial planets with $R_M < 3\,R_\oplus$, while the orange histogram is for the Jovian planets with $R_M \geqslant 3\,R_\oplus$. The red dashed vertical line is the solar slope.

One interesting aspect of Figure 4 is that the peak and overall shape of the larger mean radius subgroup is shifted to more negative slope values compared with those of the smaller mean radius subgroup. The median value of the smaller-radius subgroup is also twice as high as the larger-radius subgroup. This implies that the subgroup dominated by giant planets exhibits slightly more chemical depletion than that dominated by terrestrial planets. Intriguingly, the peak of the Jovian

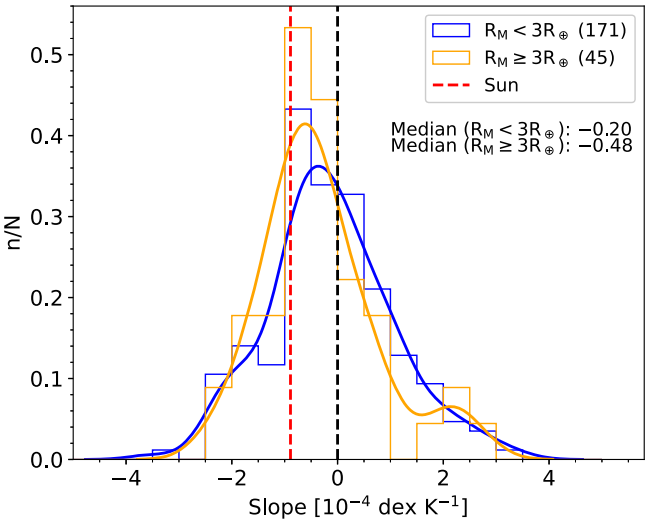

Figure 4. Distributions of the abundance–T_C slopes for two subgroups of stars, after application for GCE effects, divided by the mean radius (R_M) of the planetary system for each PHS. The blue histogram represents PHSs with $R_M < 3\,R_\oplus$, while the orange one applies to PHSs with $R_M \geqslant 3\,R_\oplus$. See Section 5.2 for details of the choice of $3\,R_\oplus$ as the dividing line. The smoothed distribution is a KDE. The median slope value for each subgroup is denoted in the legend. The red dashed vertical line is the solar slope. The distributions are normalized by the total number of stars in each subgroup.

subgroup distribution is closer to the solar slope than that of the terrestrial subgroup. Note that, according to our definition, our solar system falls into the category of the Jovian-dominated subgroup.

To further examine possible connections of the planet number and type with the chemical characteristics of their host stars, we consider the slope distributions as a function of the total radius (R_{tot}) of the planets for each PHS, as shown in Figure 5. R_{tot} is the sum of the radii of all planets that belong to a star. The top panel is the full PHS sample, while the middle and bottom panels are for the systems dominated by terrestrial and giant planets, respectively, following the same division as in Figure 4. The color code represents the number of planets in each system. The magenta symbols are the median value of the slopes in a bin of $3\,R_\oplus$ overlapped 50% with the neighboring

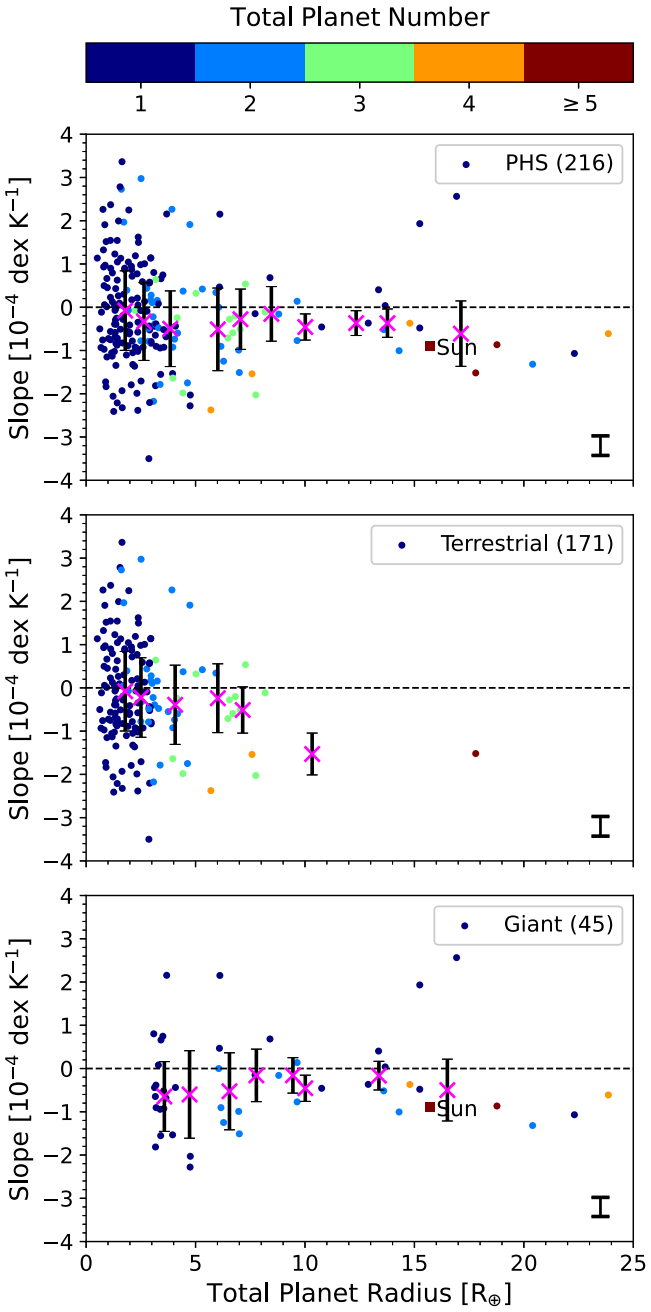

Figure 5. Elemental abundance slopes as a function of the total radius of a planetary system; $R_{\rm tot}$ is the sum of the radii of all planets that belong to a star. Our full PHS sample (top panel) is divided into terrestrial (middle panel) and giant planets (bottom panel) by the mean radius of 3 $R_\oplus$ of each planetary system. The color code indicates the total number of planets in each PHS. The magenta symbols represent the median values of slopes grouped by 3 $R_\oplus$. Each bin is overlapped with the neighboring bin by 1.5 $R_\oplus$, and the error bar is the standard deviation in each bin. Note that the rightmost bin includes all points larger than the bin value. The square in the top and bottom panels denote the Sun's slope. The typical error bar of each slope is indicated in the lower right corner in each panel.

bin, and the error bar of each PHS is the standard deviation in each bin. The typical error bar of each slope is denoted at the bottom right corner of each panel. As the Sun belongs to the Jovian-dominant subgroup in our definition, the solar slope appears in the bottom panel.

Inspection of Figure 5 reveals the following features. First, we see that most of the PHSs are dominated by a single-planet system. The top plot exhibits a tendency for having more negative slopes for $R_{\rm tot} > 5\,R_\oplus$, with more planets, indicating a greater depletion of the refractory elements. These trends can be read from the middle and bottom panels. The middle panel implies that the more rocky planets a PHS has, the more depletion of the refractory elements has taken place. In other words, the depletion trend becomes stronger as the total radius and the number of planets increase. The bottom plot also shows a small, but relatively consistent negative slope, and this tendency becomes even stronger for $R_{\rm tot} > 15\,R_\oplus$ and for more planets. However, the sample size of the giant subgroup is much smaller than that of the terrestrial subgroup, which may suffer from small number statistics. We discuss in depth the significance and implications of these findings in Section 6.3.

5.3. Number of Planets and Their Type

Figures 4 and 5 indicate that the number and type of planets may be related to the general chemical properties of their host stars. We investigate this possibility more closely in Figure 6. We divided the terrestrial group into two subgroups by the number of planets ($N_{\rm P}$) and the gas giant group according to their type. The left panel of Figure 6 represents the terrestrial group. The blue histogram is for $N_{\rm P} \leqslant 2$, while the orange histogram is for $N_{\rm P} > 2$. The smoothed curves are the kernel density estimation (KDE) of each histogram. We notice that there is a tendency for the host stars having more rocky planets to be more deficient in their refractory elements, as they exhibit more negative slopes. The median value of the slopes of the systems with $N_{\rm P} \leqslant 2$ is 5 times smaller than the systems with $N_{\rm P} > 2$. Overall, the fraction of PHSs with negative slopes is 56.8% for $N_{\rm P} \leqslant 2$, but 85.7% for $N_{\rm P} > 2$. These fractions indicate a greater depletion of the refractory elements for a star with more rocky planets.

The right panel of Figure 6 shows the slope distribution of the PHSs with the sub-Jovian (blue lines) and Jovian planets (orange lines). The division line for these two subgroups is the mean radius of 5 $R_\oplus$: sub-Jovian for $R_{\rm M} < 5\,R_\oplus$, Jovian for $R_{\rm M} \geqslant 5\,R_\oplus$. The plot clearly illustrates that the peaks between the two subgroups and the overall fraction of the PHSs with negative slopes differ significantly. The sub-Jovian subgroup has more negative slopes, demonstrating a stronger depletion of the refractory elements than for the Jovian subgroup. This suggests that the PHSs with smaller gas giants are expected to be more depleted in the refractory elements than the ones with the larger gas giants. We obtained consistent results even if we decreased the mean planet radius to $R_{\rm M} = 2\,R_\oplus$ to divide the subgroups, which is frequently used as a threshold for dividing the terrestrial planets. Our conclusion from Figures 5 and 6 is that the number and type of the planets can influence the chemical properties of their host stars. However, we also note that the sample size of the subgroups not being sufficiently large provides a strong conclusion (see Section 6.3).

6. Discussion

6.1. Correlation between Stellar Parameters and Abundance–T_C Slopes

It remains possible that the different behaviors seen in the abundance–T_C slopes between the terrestrial and giant planets may be caused by different spectral and luminosity classes of their host stars, as well as their age and metallicity. Previous studies were also concerned whether or not the magnitude and

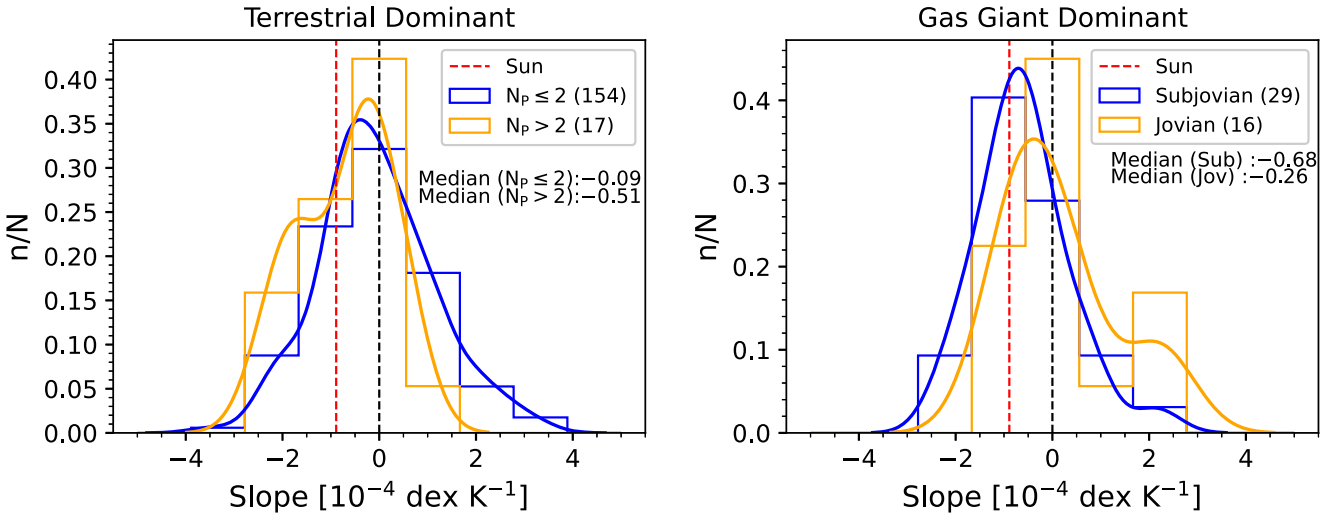

Figure 6. Left panel: distribution of the abundance slopes for the selected terrestrial planets. The planetary systems are further divided into two subgroups: one with one or two planets (blue lines) and the other with more than two planets (orange lines). The distributions are normalized by the total number of PHSs in each category. Curved lines represent the KDE of each subgroup. The median slope for each subgroup is listed in the legend. The PHSs with larger numbers of planets are shifted toward more negative slopes. Right panel: same as in the left panel, but for the sub-Jovian (blue lines) and Jovian (orange lines) subgroups. We considered the systems with $R_M < 5\ R_\oplus$ as sub-Jovian, while the one with $R_M \geqslant 5\ R_\oplus$ as Jovian.

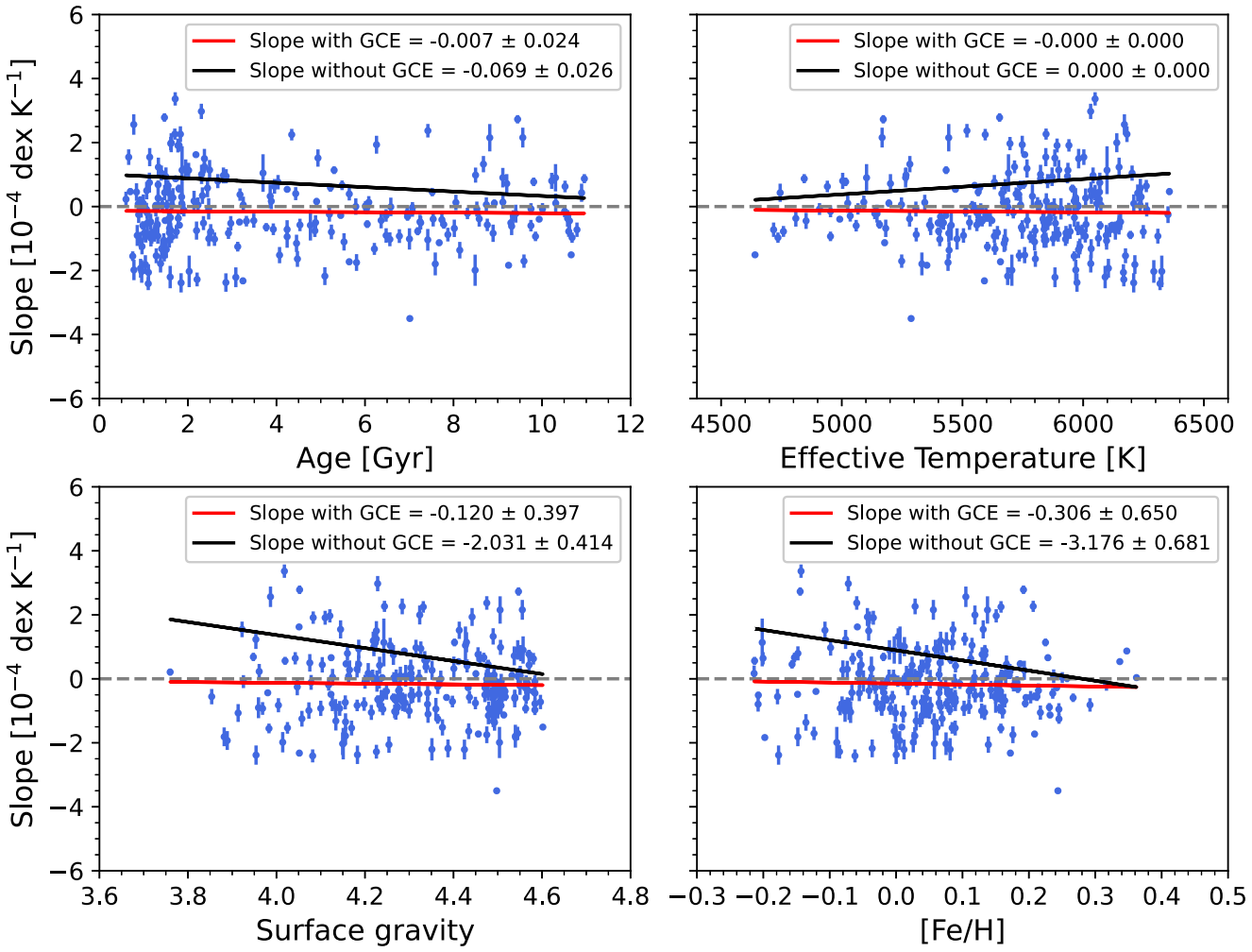

Figure 7. Abundance–T_C slopes of the PHS sample, corrected for GCE effects, as functions of the stellar parameters: age (upper left), effective temperature (upper right), surface gravity (lower left), and metallicity (lower right). The error bar on each star is calculated from 1000 random resamplings of the TPHSs for each PHS, when correcting for GCE. The red line in each panel is the linear fit to the distribution, while the black line comes from the PHSs without the GCE correction. The derived slope and its error are denoted at the top of each panel.

the sign of the abundance gradient with T_C depend on stellar parameters. For instance, Ramírez et al. (2009) reported that the abundance gradients with T_C measured by the refractory elements with $T_C > 900$ K exhibited correlations with surface gravity and metallicity, but not with effective temperature. In addition, Adibekyan et al. (2014) demonstrated that the abundance trend, regardless of the presence of the planet, had a strongly negative correlation with surface gravity and a positive correlation with stellar age. On the other hand, González Hernández et al. (2013), using 25 elements, starting from carbon with $T_C = 40$ K, could not find any correlation of their abundance slopes with the stellar temperature and metallicity. Similarly, Liu et al. (2020) claimed that there is no significant correlation between the abundance slopes of PHSs and stellar age, metallicity, or temperature with a 3σ confidence, while the NPHSs have a large scatter with the three parameters.

The present lack of consensus requires us to carefully examine possible correlations between the stellar parameters and the abundance slope in our program stars. Figure 7 shows the derived slopes of the PHSs as functions of age (upper left), effective temperature (upper right), surface gravity (lower left), and metallicity (lower right). The red line in each panel is the linear fit to the PHSs' distribution after the GCE correction, while the black line is the fit to these stars without the GCE correction. The error bar for each PHS is calculated from 1000 random resamplings of TPHSs, as in Figure 2. These plots clearly exhibit no significant trends of the abundance slopes against the various stellar parameters, after applying the GCE correction. This figure demonstrates that the disparate patterns found in the abundance slopes for the stars dominated by rocky and gas giant planets do not arise from different evolution stages, chemistry, or age of the host stars.

However, the abundance–T_C slopes of our uncorrected PHSs do exhibit negative correlations with respect to surface gravity and metallicity, and a positive correlation with effective temperature, similar to other studies that did not correct for GCE (e.g., Ramírez et al. 2009; Adibekyan et al. 2014). This once more highlights the importance of the correction of the GCE when it comes to deriving the abundance slopes. The main reason for the lack of a correlation between the abundance–T_C slope and stellar parameters may stem from the fact that, unlike previous papers applying the same GCE correction to all the samples, we selected the TPHSs sharing the same evolutionary states with each PHS to correct for the effects of GCE. It appears that our approach has removed any clear correlations with stellar parameters.

6.2. Correlation of Chemical Depletion with the Presence of Planets

We have found that the Sun exhibits a negative abundance–T_C slope of refractory elements after correcting for GCE, using twin stars in similar evolutionary states. This implies that some of the refractory elements are depleted, as reported in other previous studies (e.g., Meléndez et al. 2009; Bedell et al. 2018). It is difficult to directly compare with the literature values, because most other studies do not report the exact value of the abundance–T_C slope of the Sun. However, by reading off from their figures we carried out a qualitative assessment of our derived abundance–T_C slope, and confirmed that our value (-0.9×10^{-4} dex K^{-1}) of the Sun qualitatively agrees with other studies (e.g., Meléndez et al. 2009; Ramírez et al. 2009; Bedell et al. 2018). This similarity supports that our abundance–T_C slope, derived from six elements, can reasonably represent the slope obtained from a larger number of elements in other studies. However, Liu et al. (2020) reported an abundance–T_C slope of -0.597×10^{-4} dex K^{-1}, which is somewhat larger than ours. Nibauer et al. (2021) also reported a similar result for the solar refractory depletion as Bedell et al. (2018) from a qualitative analysis.

Our PHSs indicate a slightly lower abundance of refractory elements compared to their counterparts of TPHSs, although most of the abundance–T_C slope values of PHSs agree well with the previous results of Meléndez et al. (2009), Bedell et al. (2018), Nibauer et al. (2021), on the order of 4×10^{-4} dex K^{-1}. However, we recall that a K-S two-sample test cannot reject the null hypothesis that the PHS and TPHSs' abundance slopes are drawn from the same population, as shown in Figure 3. This argument is in line with other studies claiming very weak or no correlation between the presence of the planets and the chemical anomalies of their host stars.

As illustrated in Figures 4, 5, and 6, all terrestrial PHSs do not show refractory-element depletion; rather, some of them exhibit an enhancement of refractory elements. Some studies (e.g., Liu et al. 2020) attempted to explain the enhancement of the heavy elements as due to the engulfment of planets. That is, planetary bodies could be engulfed by their host star during its red giant phase, contributing to the higher abundance trends (Pinsonneault et al. 2001; Saffe et al. 2017; O'Connor et al. 2023; Xie et al. 2023). However, our sample of PHSs selected from APOGEE DR17 primarily consists of dwarf stars and subgiants whose evolutionary stage is too early to engulf their planets. The case of the positive slopes (or the abundance enhancements) requires more investigation.

We find that our PHSs have two unique chemical features associated with their planet populations: (1) The more rocky planets a star has, the greater the depletion of refractory elements in its host, and (2) the greater the total number of planets a star has, the more depletion of refractory elements in its host (see Figure 5). Only a few studies have attempted to explore these aspects, probably due to the limited sample size of the high-resolution spectroscopic data (Ramírez et al. 2009; González Hernández et al. 2013; Nissen 2015; Bedell et al. 2018; Mishenina et al. 2021) and the different sample-selection criteria with limited planet information (Liu et al. 2020; Tautvaišienė et al. 2022). For instance, by analyzing 24 elements from 740 bright slow-rotating stars, including 25 PHSs, Tautvaišienė et al. (2022) claimed that the metallicity of the dwarf stars hosting low-mass planets is usually high, while those with high-mass planets exhibit a greater diversity. Still, to clarify the chemical effects of the planet on the host star, additional studies with larger numbers of samples are needed.

6.3. The Impact of Planets on Chemical Anomalies of Their Host Stars

As described above, the depletion level of the refractory elements for our PHSs is correlated with their planet population. This provides us with an opportunity to relate their behavior to the suggested planet formation scenarios. Following the rocky planet argument of Meléndez et al. (2009), 60% of our samples with negative abundance slope should be depleted with refractory elements, implying the presence of rocky planets. However, because all of our PHSs do not possess rocky planets, but some of them also include giant planets, the terrestrial planets alone cannot

explain the abundance–T_C slope distribution; we need the giant planets to explain the abundance slope distributions as well. Booth & Owen (2020) showed that the pressure gap generated by forming giant planets can prevent refractory material from accreting onto their host stars. This scenario may explain the negative slope of the PHSs with large total radius planets. It follows that our findings are likely to be explained by the rocky planet theory of Meléndez et al. (2009) and the giant-planet hypothesis by Booth & Owen (2020).

Figure 6 shows a very interesting aspect of this problem, that the sub-Jovian population exhibits more negative abundance slopes than that of the Jovian population. According to the work by Hühn & Bitsch (2023), the opening gap of a protoplanetary disk from planetary formation hinders the accretion of heavy elements to the host star, leaving room for an example of a wide-binary model that explains the difference in the element-abundance ratios of each star, depending on the formation position of its giant gas planets. This model may explain the reason for the lower median abundance slope of the giant planets compared with that of the terrestrial planets seen in Figures 4 and 6. Thus, this may raise various questions about the planetary formation process of Neptune-like and Jupiter-like planets.

Our present findings cannot be solely explained by current planet formation theories. The difference in the abundances of the refractory elements between PHSs and TPHSs and the wide range of the abundance slopes may require us to take into account a variety of planet-induced effects as well. Liu et al. (2020) pointed to planet-induced effects, such as the sequestration of rocky material (depleted with refractory elements) and the engulfment of planets (enhanced with refractory elements) (Pinsonneault et al. 2001; Saffe et al. 2017; Booth & Owen 2020) for the diverse abundance trends in the PHSs. These are related to the timescale, accretion efficiency of matter, and occurrence rate of the planet formation or protoplanetary disk chemical evolution (Johansen et al. 2009; Hühn & Bitsch 2023). These effects could potentially affect the chemical composition of the PHSs seen in this study.

One of the planet-induced effects to consider to explain the diverse abundance–T_C slopes among our PHSs is the planet occurrence rate. Even though it is actively debated at present (Hsu et al. 2019), it has been reported to be as high as 1.0 (Zink et al. 2020). Microlensing studies (e.g., Cassan et al. 2012) also report a high probability for a given star to have a planet. These observational results suggest that most stars host planets that have not yet been discovered. Detecting the presence of planets by transit studies makes it difficult to discover long-period planets due to their weak signals and observational limitations. Consequently, we cannot rule out that our selected PHSs may contain more undetected planets. In turn, a high planet occurrence rate greatly complicates the identification of abundance differences among PHSs with different types of stars. Although it is unclear how much the existence of undiscovered planets influences our analysis, it is certain that, depending on the type and number of undetected planets among our PHSs, our results are subject to change.

7. Summary and Conclusions

We have analyzed a sample of PHSs selected from APOGEE DR17 to search for chemical differences compared to the TPHSs without planets. We found very weak evidence that the PHSs are more depleted with refractory elements than the TPHSs. However, we demonstrated that the amount of material contributed to planetary formation can result in the depletion of refractory elements in their host stars. Overall, the PHSs with giant planets are more depleted with heavy elements than the ones with rocky planets. Among the PHSs with rocky planets, the more rocky planets a star has, the more depletion of the refractory elements a host star exhibits. Interestingly, the sub-Jovian hosting stars exhibit more chemical depletion than the Jovian hosting stars. This may raise various questions about the planetary formation process of Neptune-like and Jupiter-like planets.

Our study indicates that the wide range of observed abundance–T_C slopes for PHSs cannot be explained solely by present planet formation scenarios; we also need to understand how planet-induced effects affect the characterization of the PHSs. Our understanding of the relationship between the elemental abundance patterns of host stars and the formation of planets is still far from complete, and many complexities remain to be unraveled. Observations with the James Webb Space Telescope (Gardner et al. 2006) should help clarify the relationship(s) between planet formation and the chemistry of host stars, with its capability to stack enormous direct infrared images of planetary systems, and test protoplanetary disk-formation theories around host stars in various stages of evolution.

Acknowledgments

Y.S.L. acknowledges support from the National Research Foundation (NRF) of Korea grant funded by the Ministry of Science and ICT (NRF-2021R1A2C1008679 and RS-2024-00333766). Y.S.L. also gratefully acknowledges partial support for his visit to the University of Notre Dame from OISE-1927130: The International Research Network for Nuclear Astrophysics (IReNA), awarded by the US National Science Foundation. T.C.B. acknowledges partial support for this work from grant PHY 14-30152; Physics Frontier Center/JINA Center for the Evolution of the Elements (JINA-CEE), and OISE-1927130: The International Research Network for Nuclear Astrophysics (IReNA), awarded by the US National Science Foundation. D.L. acknowledges support from the National Research Foundation of Korea to the Center for Galaxy Evolution Research (2022R1A6A1A03053472). Y.K. K. acknowledges the support from the Basic Science Research Program through the NRF of Korea funded by the Ministry of Education (NRF-2021R1A6A3A01086446).

Funding for the Sloan Digital Sky Survey IV has been provided by the Alfred P. Sloan Foundation, the U.S. Department of Energy Office of Science, and the Participating Institutions.

SDSS-IV acknowledges support and resources from the Center for High Performance Computing at the University of Utah. The SDSS website is www.sdss4.org. SDSS-IV is managed by the Astrophysical Research Consortium for the Participating Institutions of the SDSS Collaboration including the Brazilian Participation Group, the Carnegie Institution for Science, Carnegie Mellon University, Center for Astrophysics | Harvard & Smithsonian, the Chilean Participation Group, the French Participation Group, Instituto de Astrofísica de Canarias, The Johns Hopkins University, Kavli Institute for the Physics and Mathematics of the Universe (IPMU)/University of Tokyo, the Korean Participation Group, Lawrence Berkeley National Laboratory, Leibniz Institut für Astrophysik Potsdam (AIP), Max-Planck-Institut für Astronomie (MPIA Heidelberg), Max-Planck-Institut für Astrophysik (MPA Garching), Max-Planck-Institut für Extraterrestrische

Physik (MPE), National Astronomical Observatories of China, New Mexico State University, New York University, University of Notre Dame, Observatário Nacional/MCTI, The Ohio State University, Pennsylvania State University, Shanghai Astronomical Observatory, United Kingdom Participation Group, Universidad Nacional Autónoma de México, University of Arizona, University of Colorado Boulder, University of Oxford, University of Portsmouth, University of Utah, University of Virginia, University of Washington, University of Wisconsin, Vanderbilt University, and Yale University.

This research has made use of the NASA Exoplanet Archive, which is operated by the California Institute of Technology, under contract with the National Aeronautics and Space Administration under the Exoplanet Exploration Program.

This work presents results from the European Space Agency (ESA) space mission Gaia. Gaia data are being processed by the Gaia Data Processing and Analysis Consortium (DPAC). Funding for the DPAC is provided by national institutions, in particular the institutions participating in the Gaia MultiLateral Agreement (MLA). The Gaia mission website is https://www.cosmos.esa.int/gaia. The Gaia archive website is https://archives.esac.esa.int/gaia.

Facilities: Du Pont (APOGEE-2), Sloan (APOGEE), Gaia, Exoplanet Archive.

Software: NumPy (Harris et al. 2020), matplotlib (Hunter 2007), pandas (McKinney et al. 2010), SciPy (Virtanen et al. 2020), scikit-learn (Pedregosa et al. 2011), astropy (Astropy Collaboration et al. 2013).

ORCID iDs

Sol Yun https://orcid.org/0009-0004-1035-3309
Young Sun Lee https://orcid.org/0000-0001-5297-4518
Young Kwang Kim https://orcid.org/0000-0002-6411-5857
Timothy C. Beers https://orcid.org/0000-0003-4573-6233
Dongwook Lim https://orcid.org/0000-0001-7277-7175

References

Abdurro'uf, Accetta, K., Aerts, C., et al. 2022, ApJS, 259, 35
Adibekyan, V. Z., González Hernández, J. I., Delgado Mena, E., et al. 2014, A&A, 564, L15
Adibekyan, V. Z., Santos, N. C., Sousa, S. G., et al. 2012a, A&A, 543, A89
Adibekyan, V. Z., Sousa, S. G., Santos, N. C., et al. 2012b, A&A, 545, A32
Astropy Collaboration, Robitaille, T. P., Tollerud, E. J., et al. 2013, A&A, 558, A33
Bedell, M., Bean, J. L., Meléndez, J., et al. 2018, ApJ, 865, 68
Bedell, M., Meléndez, J., Bean, J. L., et al. 2014, ApJ, 795, 23
Behmard, A., Ness, M. K., Cunningham, E. C., & Bedell, M. 2023, AJ, 165, 178
Belokurov, V., & Kravtsov, A. 2022, MNRAS, 514, 689
Bennett, M., & Bovy, J. 2019, MNRAS, 482, 1417
Berke, D. A., Murphy, M. T., Flynn, C., & Liu, F. 2023, MNRAS, 519, 1221
Biazzo, K., D'Orazi, V., Desidera, S., et al. 2022, A&A, 664, A161
Bland-Hawthorn, J., & Gerhard, O. 2016, ARA&A, 54, 529
Booth, R. A., & Owen, J. E. 2020, MNRAS, 493, 5079
Brown, T. M., Latham, D. W., Everett, M. E., & Esquerdo, G. A. 2011, AJ, 142, 112
Cassan, A., Kubas, D., Beaulieu, J. P., et al. 2012, Natur, 481, 167
Chambers, J. E. 2010, ApJ, 724, 92
Chiba, M., & Beers, T. C. 2000, AJ, 119, 2843
Fischer, D. A., & Valenti, J. 2005, ApJ, 622, 1102
Gaia Collaboration, Montegriffo, P., Bellazzini, M., et al. 2023, A&A, 674, A33
García Pérez, A. E., Allende Prieto, C., Holtzman, J. A., et al. 2016, AJ, 151, 144
Gardner, J. P., Mather, J. C., Clampin, M., et al. 2006, SSRv, 123, 485
Gibson, B. K., Fenner, Y., Renda, A., Kawata, D., & Lee, H.-c. 2003, PASA, 20, 401
Gonzalez, G. 1997, MNRAS, 285, 403
Gonzalez, G., Carlson, M. K., & Tobin, R. W. 2010, MNRAS, 407, 314
González Hernández, J. I., Delgado-Mena, E., Sousa, S. G., et al. 2013, A&A, 552, A6
González Hernández, J. I., Israelian, G., Santos, N. C., et al. 2011, in ASP Conf. Ser. 448, 16th Cambridge Workshop on Cool Stars, Stellar Systems, and the Sun, ed. C. Johns-Krull, M. K. Browning, & A. A. West (San Francisco, CA: ASP), 879
Guerrero, N. M., Seager, S., Huang, C. X., et al. 2021, ApJS, 254, 39
Han, D. R., Lee, Y. S., Kim, Y. K., & Beers, T. C. 2020, ApJ, 896, 14
Harris, C. R., Millman, K. J., van der Walt, S. J., et al. 2020, Natur, 585, 357
Haxton, W. C., & Serenelli, A. M. 2008, ApJ, 687, 678
Heiter, U., & Luck, R. E. 2003, AJ, 126, 2015
Hsu, D. C., Ford, E. B., Ragozzine, D., & Ashby, K. 2019, AJ, 158, 109
Hühn, L. A., & Bitsch, B. 2023, A&A, 676, A87
Hunter, J. D. 2007, CSE, 9, 90
Johansen, A., Youdin, A., & Mac Low, M.-M. 2009, ApJL, 704, L75
Jönsson, H., Holtzman, J. A., Allende Prieto, C., et al. 2020, AJ, 160, 120
Kang, G., Lee, Y. S., Kim, Y. K., & Beers, T. C. 2023, ApJL, 954, L43
Kawata, D., Bovy, J., Matsunaga, N., & Baba, J. 2019, MNRAS, 482, 40
Kim, C., Lee, Y. S., Beers, T. C., & Kim, Y. K. 2023, JKAS, 56, 59
Kim, Y. K., Lee, Y. S., Beers, T. C., & Koo, J.-R. 2021, ApJL, 911, L21
Kim, Y. K., Lee, Y. S., & Beers, T. C. 2019, ApJ, 882, 176
Lee, A., Lee, Y. S., Kim, Y. K., Beers, T. C., & An, D. 2023, ApJ, 945, 56
Lee, Y. S., Beers, T. C., & Kim, Y. K. 2019, ApJ, 885, 102
Lindegren, L., Bastian, U., Biermann, M., et al. 2021, A&A, 649, A4
Liu, F., Asplund, M., Ramirez, I., Yong, D., & Melendez, J. 2014, MNRAS, 442, L51
Liu, F., Bitsch, B., Asplund, M., et al. 2021, MNRAS, 508, 1227
Liu, F., Yong, D., Asplund, M., et al. 2020, MNRAS, 495, 3961
Lodders, K. 2003, ApJ, 591, 1220
Mackereth, J. T., Bovy, J., Leung, H. W., et al. 2019, MNRAS, 489, 176
McDonough, W. F., & Sun, S. s. 1995, ChGeo, 120, 223
McKinney, W. 2010, in Proc. 9th Python in Science Conf., 445 (Austin, TX: SciPy), 51
Meléndez, J., Asplund, M., Gustafsson, B., & Yong, D. 2009, ApJL, 704, L66
Meléndez, J., Bergemann, M., Cohen, J. G., et al. 2012, A&A, 543, A29
Mishenina, T., Basak, N., Adibekyan, V., Soubiran, C., & Kovtyukh, V. 2021, MNRAS, 504, 4252
Montalbán, J., Mackereth, J. T., Miglio, A., et al. 2021, NatAs, 5, 640
Nibauer, J., Baxter, E. J., Jain, B., et al. 2021, ApJ, 907, 116
Nissen, P. E. 2015, A&A, 579, A52
Nissen, P. E. 2016, A&A, 593, A65
Nissen, P. E., Christensen-Dalsgaard, J., Mosumgaard, J. R., et al. 2020, A&A, 640, A81
O'Connor, C. E., Bildsten, L., Cantiello, M., & Lai, D. 2023, ApJ, 950, 128
Oh, S., Price-Whelan, A. M., Brewer, J. M., et al. 2018, ApJ, 854, 138
Pedregosa, F., Varoquaux, G., Gramfort, A., et al. 2011, J. Mach. Learn. Res., 12, 2825
Pignatari, M., Trueman, T. C. L., Womack, K. A., et al. 2023, MNRAS, 524, 6295
Pinsonneault, M. H., DePoy, D. L., & Coffee, M. 2001, ApJL, 556, L59
Pinsonneault, M. H., Elsworth, Y. P., Tayar, J., et al. 2018, ApJS, 239, 32
Ramírez, I., Khanal, S., Aleo, P., et al. 2015, ApJ, 808, 13
Ramírez, I., Meléndez, J., & Asplund, M. 2009, A&A, 508, L17
Saffe, C., Flores, M., & Buccino, A. 2015, A&A, 582, A17
Saffe, C., Jofré, E., Martioli, E., et al. 2017, A&A, 604, L4
Santos, N. C., Israelian, G., & Mayor, M. 2004, A&A, 415, 1153
Schönrich, R., Binney, J., & Dehnen, W. 2010, MNRAS, 403, 1829
Spina, L., Meléndez, J., Karakas, A. I., et al. 2016, A&A, 593, A125
Spina, L., Meléndez, J., Karakas, A. I., et al. 2018, MNRAS, 474, 2580
Tautvaišienė, G., Mikolaitis, Š., Drazdauskas, A., et al. 2022, ApJS, 259, 45
Teske, J. K., Khanal, S., & Ramírez, I. 2016, ApJ, 819, 19
Tucci Maia, M., Meléndez, J., & Ramírez, I. 2014, ApJL, 790, L25
Udry, S., & Santos, N. C. 2007, ARA&A, 45, 397
Virtanen, P., Gommers, R., Oliphant, T. E., et al. 2020, NatMe, 17, 261
Wang, H. S., Quanz, S. P., Yong, D., et al. 2022, MNRAS, 513, 5829
Xie, D., Zhu, C., Guo, S., Liu, H., & Lü, G. 2023, MNRAS, 524, 3705
Zink, J. K., Hardegree-Ullman, K. K., Christiansen, J. L., et al. 2020, AJ, 160, 94